electronic materials

MDPI

Article

p-Type Iodine-Doping of Cu_3N and Its Conversion to γ-CuI for the Fabrication of γ-CuI/Cu_3N p-n Heterojunctions

Argyris Tilemachou [1], Matthew Zervos [1,*], Andreas Othonos [2], Theodoros Pavloudis [3] and Joseph Kioseoglou [3]

[1] Nanostructured Materials and Devices Laboratory, School of Engineering, University of Cyprus, P.O. Box 20537, Nicosia 1678, Cyprus; argyristilemachou@gmail.com
[2] Laboratory of Ultrafast Science, Department of Physics, School of Sciences, University of Cyprus, P.O. Box 20537, Nicosia 1678, Cyprus; othonos@ucy.ac.cy
[3] Department of Physics, Aristotle University of Thessaloniki, GR-54124 Thessaloniki, Greece; tpavlo@auth.gr (T.P.); sifisl@auth.gr (J.K.)
* Correspondence: zervos@ucy.ac.cy

Abstract: Cu_3N with a cubic crystal structure is obtained in this paper by the sputtering of Cu under N_2 followed by annealing under NH_3: H_2 at 400 °C, after which it was doped with iodine at room temperature resulting into p-type Cu_3N with hole densities between 10^{16} and 10^{17} cm^{-3}. The Cu_3N exhibited distinct maxima in differential transmission at ~2.01 eV and 1.87 eV as shown by ultrafast pump-probe spectroscopy, corresponding to the M and R direct energy band gaps in excellent agreement with density functional theory calculations, suggesting that the band gap is clean and free of mid-gap states. The Cu_3N was gradually converted into optically transparent γ-CuI that had a hole density of 4×10^{17} cm^{-3}, mobility of 12 cm^2/Vs and room temperature photoluminescence at 3.1 eV corresponding to its direct energy band gap. We describe the fabrication and properties of γ-CuI/TiO_2/Cu_3N and γ-CuI/Cu_3N p-n heterojunctions that exhibited rectifying current-voltage characteristics, but no photogenerated current attributed to indirect recombination via shallow states in Cu_3N and/or deep states in the γ-CuI consistent with the short (ps) lifetimes of the photoexcited electrons-holes determined from transient absorption–transmission spectroscopy.

Keywords: copper nitride; copper iodide; semiconductors; p-type doping; p-n heterojunctions

Citation: Tilemachou, A.; Zervos, M.; Othonos, A.; Pavloudis, T.; Kioseoglou, J. p-Type Iodine-Doping of Cu_3N and Its Conversion to γ-CuI for the Fabrication of γ-CuI/Cu_3N p-n Heterojunctions. *Electron. Mater.* **2022**, *3*, 15–26. https://doi.org/10.3390/electronicmat3010002

Academic Editor: Michele Goano

Received: 4 November 2021
Accepted: 4 January 2022
Published: 10 January 2022

1. Introduction

Cu_3N is an indirect energy band gap semiconductor, in which crystal imperfections, such as N vacancies (V_N) and Cu interstitials (Cu_i), do not give rise to mid-gap states, but instead electronic states that are energetically located very close or inside the conduction and valence band edges, respectively. Consequently, it has been described as a defect tolerant semiconductor and proposed to be used as an absorber material for the fabrication of p-n junction solar cells [1], considering that n- and p-type doping is also possible. Furthermore, it has an anti-ReO_3 cubic crystal structure in which ions can be stored at its center making it suitable for batteries so it is still an active topic of investigation for energy conversion and storage [2].

In the past, Cu_3N has been obtained mostly by reactive sputtering of Cu under N_2 in conjunction with Ar, which enables control over its stoichiometry. For instance, Birket et al. [3] prepared Cu_3N by sputtering of Cu under Ar and N_2, but recently we obtained Cu_3N from Cu on fused SiO_2 (f-SiO_2) under a flow of NH_3: O_2 between 400 °C and 600 °C similar to Matsuzaki et al. [4]. Interestingly, we observed the M and R direct energy band gaps of Cu_3N by ultra-fast pump-probe spectroscopy (UPPS) [5], confirming that Cu_3N has a "clean" energy band gap with no mid-gap states. Whille there are many investigations on n-type doping of Cu_3N, only a few have considered p-type doping, such as the one conducted by Matsuzaki et al. [4] who showed that p-type Cu_3N can be obtained

via the incorporation of interstitial F. Alternatively, S and Se can be used to control the carrier type [6,7].

To the best of our knowledge, no one has investigated the properties of I: Cu_3N and its gradual conversion into γ-CuI despite the fact that Cu_3N has been converted into γ-CuI previously by exposure to iodine in a one-step process [8,9]. One of the advantages of using iodine is that it has a low melting point of 114 °C and a corresponding high vapor pressure of 10 kPa, but more importantly it is not so toxic compared to fluorine. Moreover, the ability to obtain p-type Cu_3N by doping with iodine is not just interesting from a fundamental point of view, but also important for the realization of p-n homojunction solar cells, e.g., by selective compensation of n-type Cu_3N. Furthermore, the conversion of Cu_3N into γ-CuI is important for the realization of devices as γ-CuI is a highly transparent, p-type semiconductor, with a direct energy band gap of 3.2 eV that has been used extensively in perovskite solar cells [10], organic solar cells [11], dye sensitized [12], silicon solar cells [13], light emitting diodes [14], transistors [15], and thermoelectric devices [16]. Consequently, one may obtain p-n heterojunctions [17–19] using p-type γ-CuI in conjunction with n-type Cu_3N.

It is important to emphasize that, although Cu_3N has been described to be a defect tolerant semiconductor that is attractive as a solar cell absorber, no one as yet has actually fabricated a working p-n junction solar cell using Cu_3N. In the past, Chen et al. [20] fabricated a p-n Cu_3N homo junction on indium tin oxide (ITO) and Yee et al. [21] fabricated an Al: ZnO/ZnS/Cu_3N p-n heterojunction, both of which showed rectifying behavior, but no photo generated current. On the other hand, however, Yu et al. [22] fabricated Ag/Cu_3N/ITO and Ag/Mn: Cu_3N/ITO devices that had a high photocurrent response and exhibited linear IV characteristics in the dark and light, but they did not fabricate a p-n junction exhibiting rectifying properties and photovoltaic action.

In this paper, we consider the structural, electrical and optical properties of I: Cu_3N and γ-CuI in conjunction with density functional theory (DFT) calculations of the electronic band structure in order to advance our understanding of these semiconductors and also show how p-type γ-CuI and n-type Cu_3N may be combined to form γ-CuI/Cu_3N p-n heterojunctions exhibiting rectifying current-voltage characteristics.

2. Materials and Methods

2.1. Experimental Proceedure

Initially, 60 nm of Cu_3N was deposited on f-SiO_2 by reactive sputtering of a Cu target using pure N_2 at 10^{-2} mbar. The Cu_3N was subsequently annealed at 400 °C for 30 min under 300 mL/min of NH_3 and 15 mL/min H_2 using a ramp rate of 30 °C/min in order to improve its crystal quality. The doping and gradual conversion of Cu_3N into γ-CuI_2 was carried out using 10 mg of iodine (I_2) inside a Petri dish at room temperature for 20 up to 200 s.

The morphology, composition and crystal structure of the I: Cu_3N and γ-CuI were investigated by scanning electron microscopy (SEM, Tescan, Brno, Czech Republic), energy dispersive X-ray analysis (EDX) and X-ray diffraction (XRD) (Rigaku Mini Flex).

The electrical properties were measured by the Hall effect in the van der Pauw geometry at room temperature using a 0.5 T GMW 3470 electromagnet in conjunction with a Keithley 2635A constant current source, 2182 Nano voltmeter (Keithley, Cleveland, OH, USA).

The optical properties and in particular the time evolution of the differential transmission (dT/T) through the I: Cu_3N and γ-CuI deposited on f-SiO_2 were measured on a ps time scale in a typical pump–probe configuration using a pump of λ_{PU} = 400 or 260 nm and a probe that varied between λ_{PR} = 450 nm and 750 nm, as described in detail previously [5]. For completeness, the photoluminescence (PL) of the γ-CuI was measured between 77 and 300 K. The PL was measured using a coherent, high repetition rate ultrafast amplifier, centered at 800 nm that generated 75 fs pulses at 250 kHz. The fundamental light at 800 nm was tripled at 266 nm using barium borate crystals. The sample was loaded in a Janis closed cycle refrigerator and the PL emission was directed into an Andor spectrometer equipped with an iStar intensified CCD camera.

2.2. Theoretical

The density functional theory (DFT) calculations were performed using the Vienna Ab initio Simulation Package (VASP) [23,24] with Projector Augmented-Wave (PAW) pseudopotentials [25,26] using Perdew–Burke–Ernzerhof Generalized Gradient Approximation functionals (PBE-GGA) [27]. The DFT + U method was employed via the approach introduced by Dudarev et al. [28]. The +U potential was applied only to the d electrons of Cu and the U_{eff} parameter was set at 7.64 eV, which is a value that was found to accurately reproduce the experimental bandgap of Cu_3N [5]. The energy cut-off of the plane-wave basis set was 520 eV. We used 5 × 5 × 5 500-atom cubic Cu_3N, fully relaxed supercells, for the calculations and the Brillouin zone was sampled using a Γ-centred 2 × 2 × 2 mesh. The defect formation energies were calculated according to the methodology described by Freysoldt et al. [29]. For Cu-rich conditions, the chemical potential of Cu was assumed to be $\mu_{Cu} = E_{Cu,bulk}$ and consequently the chemical potentials of N and I were calculated by $\mu_N = E_{Cu_3N,bulk} - \mu_{Cu}$ and $\mu_I = E_{CuI,bulk} - \mu_{Cu}$, which were also for N-rich and I-rich conditions, where the energies of the N_2 dimer, pyramidal I_3N molecules and I in its orthorhombic phase were taken into account.

3. Results

3.1. Structural, Electrical and Optical Properties of p-Type I: Cu_3N and γ-CuI

Initially, Cu_3N was deposited by reactive sputtering of Cu under pure N_2 on f-SiO_2 for the purpose of measuring the optical and electrical properties, but the f-SiO_2 was not heated during the deposition. The Cu_3N layers obtained in this way did not exhibit any distinct peaks in the XRD suggesting a poor crystal quality, so they were annealed under NH_3: H_2 at 400 °C for 30 min in order to improve their crystallinity and a typical SEM image is shown in Figure 1a. The Cu_3N layers exhibited well resolved peaks after annealing corresponding to the cubic crystal structure of Cu_3N as shown in Figure 1b. As expected, we did not detect any peaks related to CuO or Cu_2O as we included H_2 along with the NH_3.

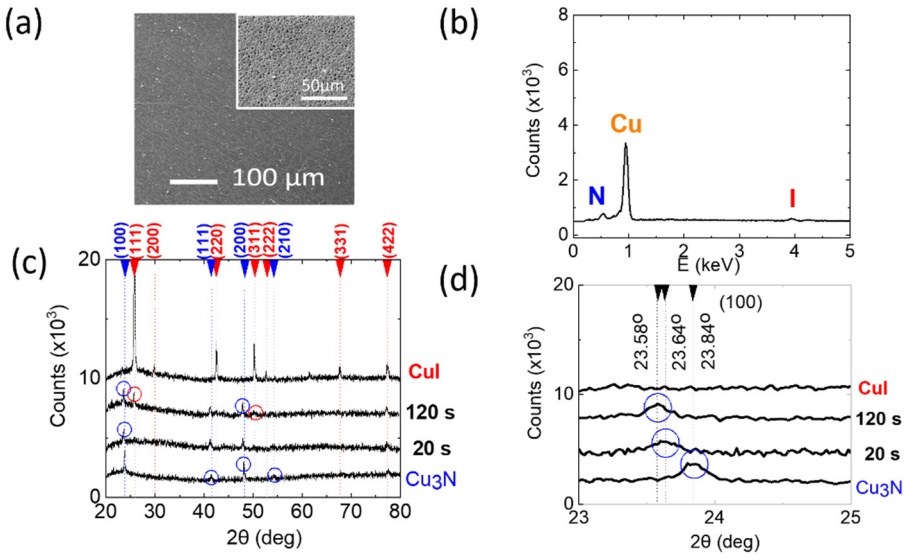

Figure 1. (**a**) SEM image of Cu_3N after annealing at 400 °C for 30 min under NH_3: H_2; inset shows γ-CuI after the complete conversion of Cu_3N under I_2 for 200 s. (**b**) XRD traces obtained from Cu_3N after annealing, i.e., bottom trace, and I: Cu_3N obtained by iodization for 20 s and 120 s; top trace corresponds to γ-CuI. (**c**) EDX of I: Cu_3N and (**d**) section of XRD between 2θ = 23 and 25° showing the shift of the (100) peak of Cu_3N that occurs upon the incorporation of iodine corresponding to a strain of ~1%.

The ability to obtain n- and p-type Cu_3N via the incorporation of specific impurities is an attractive feature of Cu_3N that is important for the realization of p-n junction solar cells.

Recently, Matzusaki et al. [4] showed that p-type Cu_3N layers with a room temperature hole density between 10^{16}–10^{17} may be obtained via the intentional incorporation of F. Another way to obtain p-type Cu_3N is via the incorporation of iodine. Consequently, p-type Cu_3N layers were obtained by the exposure of the Cu_3N layers to iodine for 20 s at room temperature. This did not change the surface morphology of the Cu_3N, which looked very similar to that in Figure 1a. The incorporation of iodine for 20 s resulted into the formation of p-type Cu_3N with a hole density of 2×10^{16} cm^{-3} and mobility of 24 cm^2/Vs, but we did not observe the formation of γ-CuI alongside Cu_3N, as shown by the XRD in Figure 1b. We found that the hole density increased from 2×10^{16} cm^{-3} to 6×10^{16} cm^{-3} and then 1.1×10^{17} cm^{-3} by increasing the exposure of the Cu_3N layer to iodine from 20 to 60 and 100 s, respectively, at room temperature. These hole densities did not change after a 24 h long exposure to the ambient. We find that the extended incorporation of iodine in Cu_3N at room temperature over 120 s resulted in the formation of γ-CuI alongside Cu_3N as shown in Figure 1b. Now, γ-CuI has a zinc blended crystal structure, with a lattice constant of a = 0.608 nm. In contrast, the Cu_3N has a cubic crystal structure with a lattice constant of a = 0.38 nm. As such, the conversion of certain regions of Cu_3N into γ-CuI will result into a significant expansion of the lattice imposing strain on the Cu_3N. This is manifested by the gradual shift of the (100) peak of Cu_3N shown in Figure 1d that occurs upon the incorporation of iodine. An overall shift of -0.26° is observed that is nearly identical to the shift of $2\theta = -0.28^\circ$ observed in the case of the (200) peak of Cu_3N and that corresponds to a strain of ~1%. The Cu_3N was eventually converted into γ-CuI, as shown by the suppression of the peaks belonging to Cu_3N in the trace at the top of Figure 1b. It should be noted here that the conversion of Cu into γ-CuI involves the oxidation of Cu from Cu^0 to Cu^{+1}. In contrast, the conversion of Cu_3N into CuI just involves the replacement or substitution of N with I given that Cu_3N is composed of Cu^{+1} and N^{+3}. This reaction occurs at room temperature so the Cu_3N may be gradually converted into an optically transparent γ-CuI in a highly controllable fashion. A typical SEM image of the γ-CuI obtained from Cu_3N after complete conversion over 200 s is shown as an inset in Figure 1a. The γ-CuI had a hole density of 4×10^{17} cm^{-3} and mobility of 12 cm^2/Vs, which falls in the range 0.5–50 $cm^2/V{\cdot}s$ [10,14] of hole mobilities found previously for γ-CuI. In addition to measuring the structural and electrical properties of the I: Cu_3N and γ-CuI, we also measured their optical properties by UPPS. The I: Cu_3N exhibited distinct spectral features at ~660 nm (≡1.87 eV) and 617 nm (≡2.01 eV) as measured by UPPS and shown in Figure 2a,b. These correspond to the M and R direct energy band gaps of bulk-relaxed Cu_3N similar to what we have observed previously for Cu_3N obtained from Cu under NH_3: O_2 [5], but here we do not observe the duo of higher energy peaks that were recently attributed to the formation of strained Cu_3N arising in connection with surface oxidation upon exposure to the ambient [30].

However, the extended incorporation of iodine for 120 s lead to the emergence of an additional maximum in differential transmission at ~420 nm (≡2.95 eV), as shown in Figure 2c,d. The higher energy maximum observed in Figure 2d is not related to γ-CuI itself, but to the emergence of strained regions of Cu_3N due the lattice expansion of γ-CuI as explained above. We find that the total conversion of Cu_3N into γ-CuI leads to a suppression of all the maxima shown in Figure 2 and the emergence of a single maximum in differential transmission at ~420 nm (≡2.95 eV), as shown in Figure 3a,b. This sharp peak at ~420 nm (≡2.95 eV) is consistent with the direct energy band gap of γ-CuI, which is an optically transparent p-type semiconductor. Given that Cu_3N is an indirect gap semiconductor, it shows no PL, but the γ-CuI is a direct gap semiconductor that exhibited PL at 3.1 eV and also a broad emission between 1.55–2.06 eV (≡800–600 nm) at room temperature, as shown in Figure 3c,d. The PL at 3.1 eV is attributed to band-to-band radiative recombination of photo excited electron hole pairs, as shown in Figure 4a, while the broad emission is attributed to radiative recombination via mid gap states, as shown in Figure 4c. In addition, we found that the γ-CuI shows PL at 825 nm (≡1.5 eV), also shown

in Figure 3c. The red PL at 1.5 eV has been shown to be related to iodine vacancies, as illustrated in Figure 4d, and is not an artifact related to the PL at 400 nm.

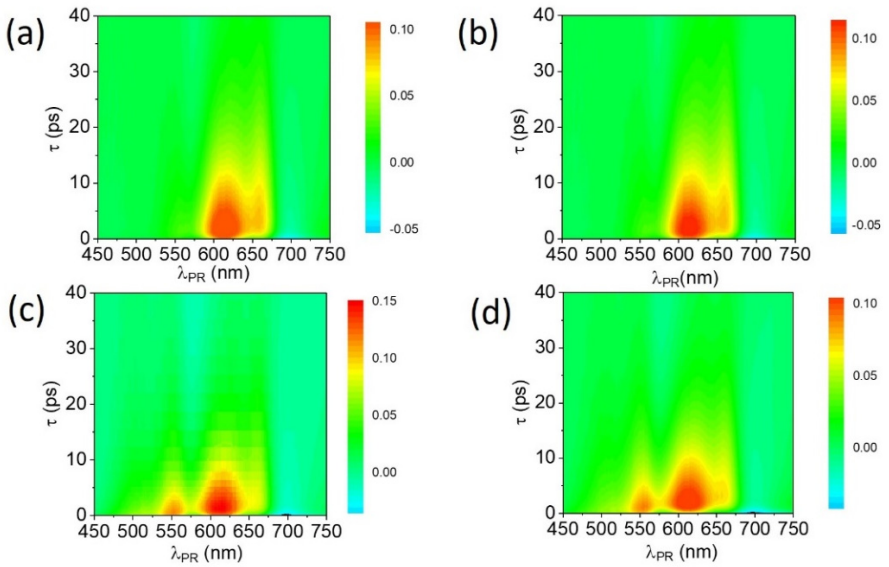

Figure 2. UPPS of Cu_3N layer after doping with iodine for different times showing differential transmission (dT/T) versus optical delay τ(ps) for different λ_{PR} (nm) (**a**) for 20 s with λ_{PU} = 400 nm, (**b**) for 20 s with λ_{PU} = 260 nm, (**c**) for 120 s with λ_{PU} = 400 nm, and (**d**) for 120 s with λ_{PU} = 260 nm. Maxima at ~1.87 eV (660 nm), 2.01 eV (617 nm) and 2.25 eV (550 nm); in all cases the vertical color bar corresponds to the differential transmission dT/T.

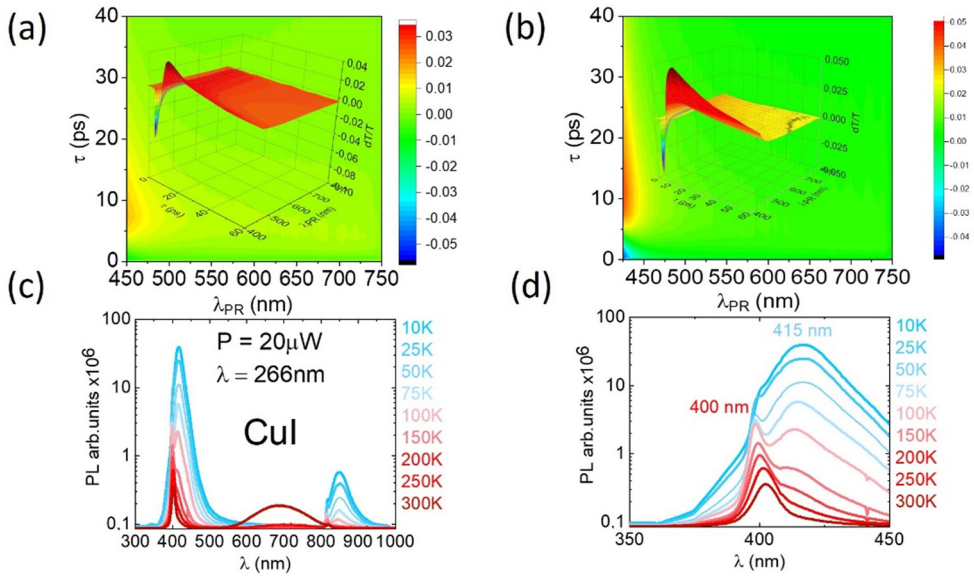

Figure 3. UPPS of γ-CuI with λ_{PU} = 266 nm and 5 μJ at (**a**) 300 K and (**b**) 77 K; maximum at ~2.95 eV (≡420 nm); vertical color bar corresponds to the differential transmission dT/T and the insets show the corresponding three-dimensional graph. Moreover, the figure also shows (**c**) the PL from γ-CuI taken with an excitation of λ_{PU} = 266 nm between 10 and 300 K and (**d**) PL from γ-CuI between 350 and 450 nm.

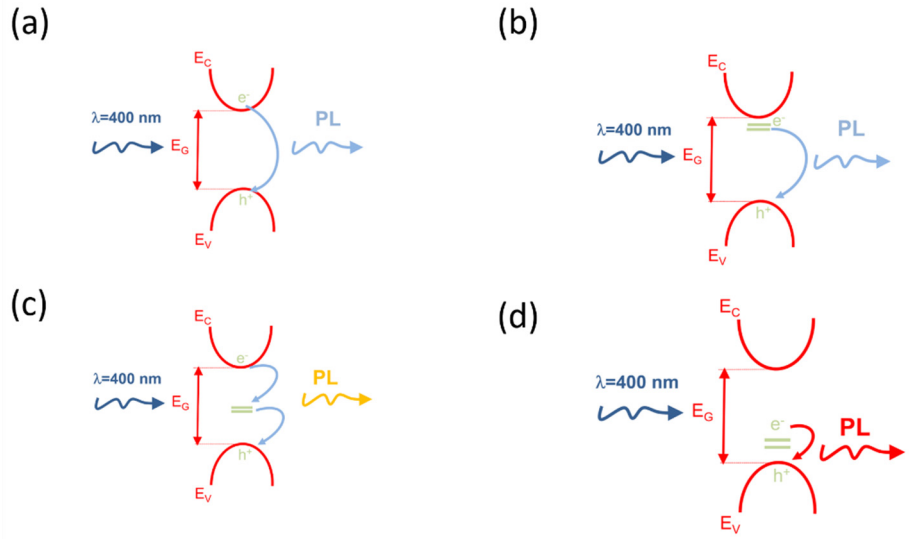

Figure 4. Schematic diagram of (**a**) band-to-band radiative recombination of photo excited electron hole pairs related to the PL at 3.1 eV in γ-CuI; (**b**) radiative recombination via shallow donor-like states giving rise to the PL at 3.0 eV in γ-CuI; (**c**) recombination via mid-gap states; and (**d**) radiative recombination of photo excited electron hole pairs via acceptor-like states related to iodine vacancies (V_I) in γ-CuI.

For completeness, we ought to point out that the PL intensities at ~3.1 eV and ~1.5 eV increased by reducing the temperature from 300 to 77 K, but this also resulted in a suppression of the broad PL observed between 1.55 and 2.06 eV. However, we observed the emergence of a local maximum in the PL at 415 nm (≡3.0 eV), as shown in Figure 3d, which is attributed to radiative recombination via donor-like vacancies, as explained in Figure 4b.

3.2. DFT Electronic Band Structure Calculations

In order to further understand all of the above findings, we investigated the formation energies of the iodine defects and their effect on the electronic band structure of Cu_3N via large-scale ab initio calculations. We considered I in two interstitial and two substitutional positions in the simple cubic anti-ReO_3 phase structure of Cu_3N (space group $Pm\bar{3}m$, No. 221), i.e., the following four configurations: (**a**) $I_{i,1b}$: an I atom in the single 1*b* Wyckoff position (in the center of the cube defined by the Cu and N atoms, fractional coordinates: 0.5 0.5 0.5); (**b**) $I_{i,3c}$: an I atom in one of the 3c Wyckoff positions (in the center of a facet the cube defined by the Cu and N atoms, fractional coordinates: 0.5 0.5 0.0); (**c**) I_{Cu}: an I atom in the place of a Cu atom; and (**d**) I_N: an I atom in the place of a N atom, with Cu and N atoms occupying the 3d and the single 1a sites respectively, shown in Figure 5.

We found that $I_{i,1b}$ is energetically preferable under both Cu-rich and N-rich conditions for all the different types of potentials used. Both $I_{i,1b}$ and I_{Cu} show lower formation energies under N-rich conditions (1.41 eV down from 3.31 eV and 1.73 eV from 3.44, respectively). The barrier for an I atom to diffuse from one 1b position to the neighboring is ~1.6–1.8 eV depending on the conditions. Under I-rich conditions I_{Cu} is preferable and shows a formation energy of 1.83 eV compared to 2.51 eV of $I_{i,1b}$. The formation energy of $I_{i,3c}$ and I_N are always high (3.03 eV and 5.84 eV for N-rich conditions respectively).

The formation energies of all the defects in Cu_3N as a function of the Fermi energy are shown in Figure 5. The interstitial defect induces 1 acceptor level at 0.08 eV, where the transition from the 0 charge to −1 charge happens. One additional level is found right at the conduction band minimum (CBM) for the transition from −1 to −2 charge. One non-visible in the figure transition level is −0.01 eV below the valence band maximum (VBM), where the transition from the +1 charge to 0 charge takes place (not shown in the figure). The substitutional defect I_{Cu} is always uncharged. In addition to the above, we also calculated the formation energies of the Cu_i, V_{Cu} and V_N native point defects, which

are in good agreement with the formation energies calculated by Matsuzaki et al. [4], i.e., Cu_i: ~0.7 eV, V_{Cu}: ~1.1 eV and V_N: ~2.4 eV.

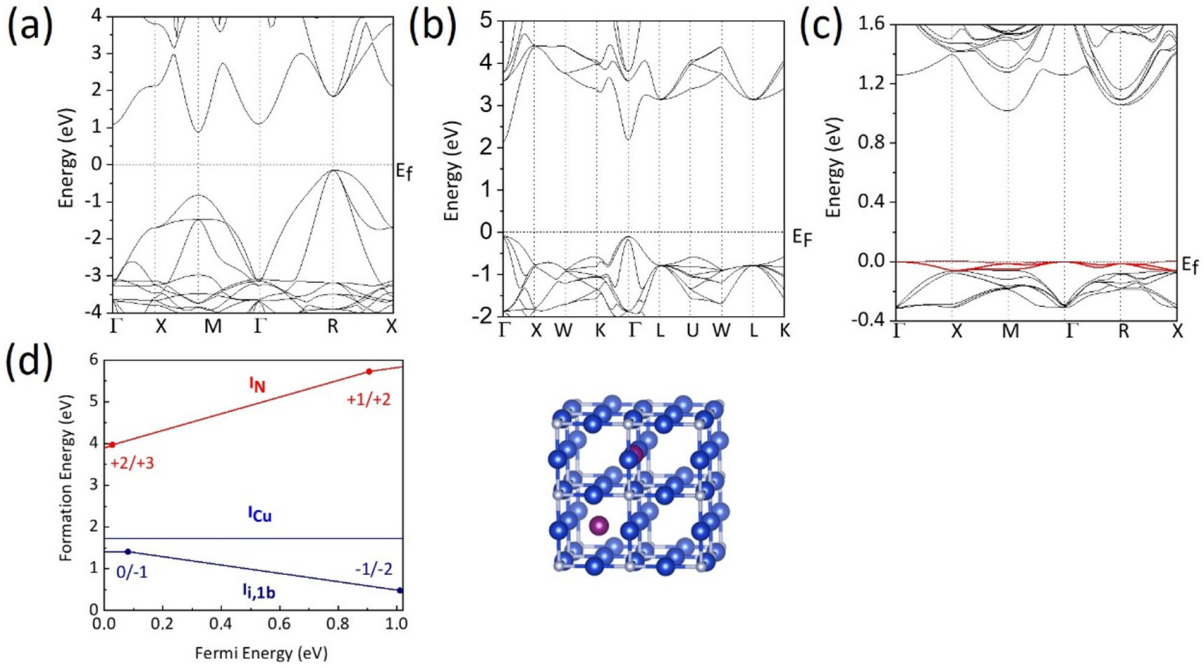

Figure 5. (**a**) Electronic band structure of intrinsic Cu_3N showing the M and R direct band gaps as well as the M to R indirect energy band gaps. (**b**) Electronic band structure of intrinsic CuI showing the Γ direct band gap. (**c**) Electronic band structure of I: Cu_3N derived using one iodine atom per 375 Cu atoms and 125 N atoms; the red line corresponds to the shallow acceptor like states of iodine. (**d**) Formation energies and charge-state transition points of the I-related defects in Cu_3N under N-rich conditions as a function of the Fermi energy. The minimum and the maximum of the Fermi energy correspond to the valence band maximum and conduction band minimum, respectively. Solid lines correspond to the formation energy and only the most energetically favourable charge state for a specific Fermi energy is shown. Positive and negative charge states indicate donor and acceptor behaviour, respectively; also shown the crystal structure of Cu_3N showing the large Cu and small N atoms as well as the interstitial positions of the I atoms.

For completeness, the electronic band structure of Cu_3N, γ-CuI and I: Cu_3N is shown in Figure 5a–c. We found that the incorporation of iodine yields states that are energetically located very close to the conduction band minimum and valence band maximum leaving a "clean" band gap very similar to the findings of Yee et al. [21] who showed that N vacancies (V_N) and Cu interstitials (Cu_i) give rise to states that are energetically located very close or inside the conduction and valence band edges. In other words, I: Cu_3N has a "clean" band gap, thus allowing the observation of the maxima at 617 nm (≡2.01 eV) and 660 nm (≡1.87 eV) by UPPS, which unequivocally correspond to the M and R direct energy band gaps of Cu_3N.

3.3. γ-CuI/TiO_2/Cu_3N and γ-CuI/Cu_3N p-n Heterojunctions

Initially, we fabricated a γ-CuI/TiO_2/Cu_3N p-n heterojunction on soda lime glass (SLG), as shown in Figure 6. First, a 100 nm layer of Au was deposited by sputtering under Ar at 10^{-2} mbar on 15 mm × 25 mm SLG, which was used as a back contact. Following this, a 100 nm layer of n-type Cu_3N layer was deposited over the Au by reactive sputtering under Ar: 10%N_2 and annealed under NH_3: H_2 at 400 °C for 30 min in order to improve its crystal quality. Subsequently, a 10 nm thick TiO_2 layer was deposited by reactive sputtering under Ar: 10% O_2. This is usually annealed at elevated temperatures, e.g., 500 °C, in air or under oxygen in order to improve its crystal quality and eliminate mid-gap states, but

we avoided doing so in order to prevent the degradation of the underlying n-type Cu_3N. Finally, a Cu_3N layer was deposited by reactive sputtering on top of the TiO_2 using a Cu target under 100% N_2, which was converted into γ-CuI by an extended iodization of 200 s at room temperature. The device was completed with the deposition of a 100 nm thick Au contact on top of the γ-CuI. The IV characteristics of the devices were measured at room temperature with a Keithley 2635A.

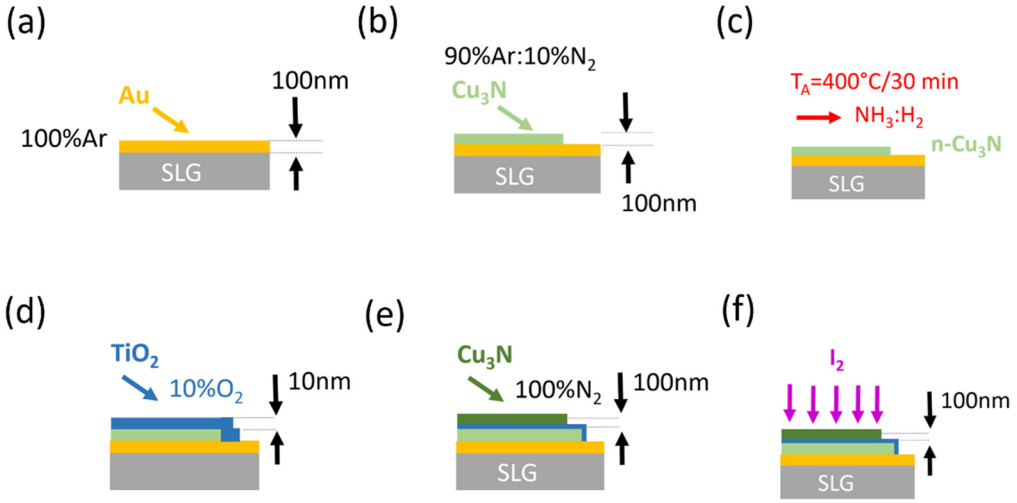

Figure 6. Schematic diagram showing the fabrication of the γ-CuI/TiO_2/Cu_3N p-n heterojunction: (**a**) deposition of 100 nm Au on SLG; (**b**) deposition of n-type Cu_3N; (**c**) annealing at 400 °C/30 min under NH_3:H_2; (**d**) deposition of 10 nm TiO_2 barrier by reactive sputtering under Ar: 10% O_2; and (**e**) sputtering of N-rich Cu_3N (**f**) conversion of N-rich Cu_3N into γ-CuI.

Before considering the IV properties of the γ-CuI/TiO_2/Cu_3N p-n heterojunction, it is useful to point out that γ-CuI is a p-type semiconductor with an energy band gap of 3.2 eV that has a work function of ϕ = 5.0 eV and a small electron affinity of χ = 2.1 eV, as shown in Figure 7a [14,31,32]. In contrast, the electron affinity and work function of n-type Cu_3N are χ = 3.5 eV and ϕ =4.0 eV, respectively, as shown in Figure 7b. Furthermore, TiO_2 has a band gap of 3.2 eV, work function of ϕ =4.2 eV and an electron affinity of χ = 4.0 eV, as shown in Figure 7c, making it attractive as a barrier. These properties are expected to induce strong band bending and a substantial built-in barrier in a γ-CuI/TiO_2/Cu_3N p-n heterojunction, as shown in Figure 7d. The γ-CuI/TiO_2/Cu_3N p-n heterojunction exhibited a strongly asymmetric current-voltage (IV) characteristic, as shown in Figure 7e, with an on–off ratio of ~34 and were stable under ambient conditions. The Au on top of the γ-CuI as well as Au on n-type Cu_3N results into the formation of ohmic contacts, as we obtained linear IV characteristics from a single layer of (a) γ-CuI and (b) n-type Cu_3N that were deposited separately on SLG, as shown in Figure 8a,b. The n-type Cu_3N had an electron density of n = 1.2 × 10^{18} cm^{-3} and mobility of 1.6 cm^2/Vs due to the fact that it was deposited under Cu-rich conditions, i.e., under Ar: 10% N_2. In addition to Au, one could use Ag as well as Cu on n-type Cu_3N, which also exhibited linear IV characteristics. However, it should be emphasized that Ag on top of γ-CuI leads to non-linear IV characteristics consistent with the fact that CuI/AgI is a p-n heterojunction, in itself with rectifying properties. Consequently, Ag was not used as an ohmic contact to γ-CuI in the case of the γ-CuI/TiO_2/Cu_3N p-n heterojunction.

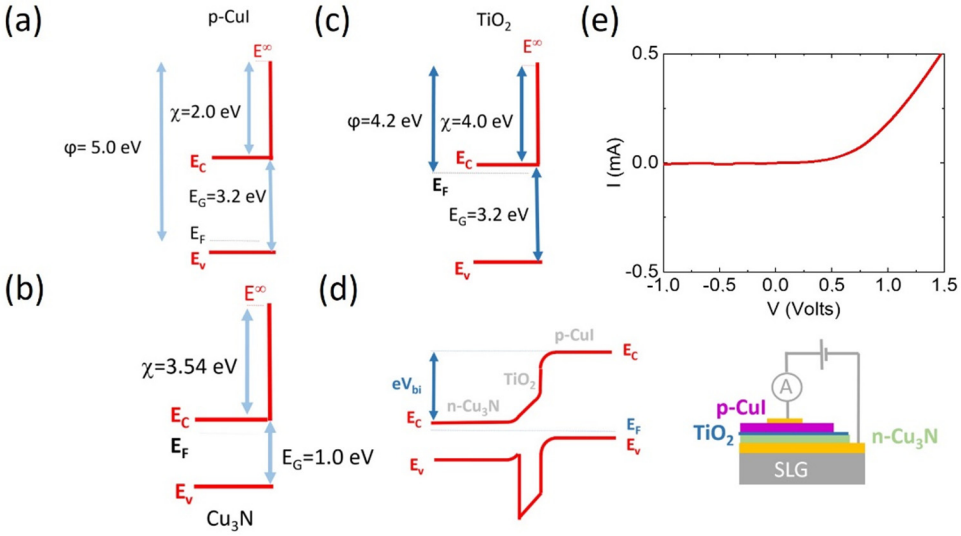

Figure 7. Schematic energy band diagram of (**a**) γ-CuI (**b**) Cu_3N and (**c**) TiO_2 showing the energy band gap, electron affinity χ and work function ϕ. The diagram also shows the (**d**) band profile of γ-CuI/TiO_2/Cu_3N p-n heterojunction and (**e**) the IV characteristic obtained from the γ-CuI/TiO_2/Cu_3N p-n heterojunction at room temperature.

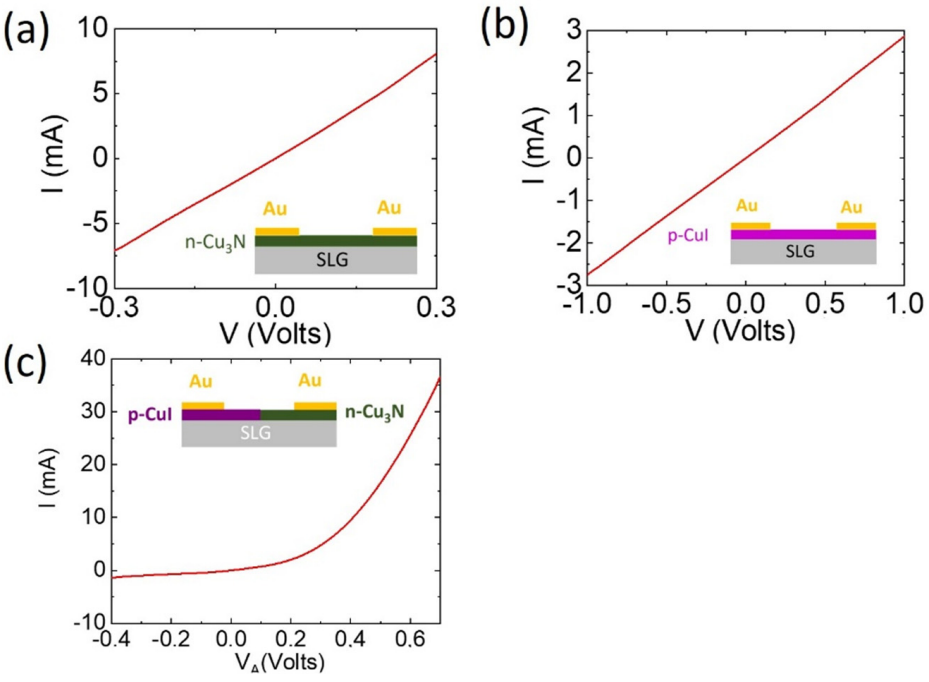

Figure 8. Schematic diagram and IV characteristics obtained from (**a**) Au contacts on n-type Cu_3N, (**b**) Au contacts on p-type γ-CuI and (**c**) γ-CuI/Cu_3N p-n planar heterojunction with Au contacts. The Cu_3N, γ-CuI as well as the Au contacts had a thickness of 100 nm.

It is also important to point out that the IV characteristics obtained from a symmetric Au/TiO_2/Au device, which in essence constitutes a single tunnel barrier, are non-linear, but nevertheless symmetric. Evidently, the rectifying IV characteristic shown in Figure 7e is related solely to the formation of the p-n heterojunction between the p-type γ-CuI and n-type Cu_3N layer. One could argue that the rectifying IV characteristics are attributed to the formation of a p-n junction between the p-type CuI and n-type TiO_2, as suggested by Kumarasinghe et al. [33]. However, the TiO_2 layer in our device is very thin, i.e., 10 nm, so it will be essentially depleted, and it is impossible for such a thin TiO_2 layer to contain

a depletion region and electric field as well as a flat band region so that the rectifying properties of the device are attributed to the CuI/TiO_2 p-n junction. This would require a very high electron density in the TiO_2, well in excess of the electron density that can exist in such an un-doped, wide band gap oxide, such as TiO_2. In other words, the TiO_2 layer acts as a tunnel barrier and the rectifying properties are strictly related to the p-type CuI and n-type Cu_3N. More specifically, the application of a forward bias, i.e., externally applied electric field to the γ-CuI/TiO_2/Cu_3N p-n heterojunction that is opposite to the built-in electric field that points from the n-type Cu_3N to the p-type γ-CuI, will reduce the built-in barrier. This will allow electrons to frow from the n-type Cu_3N to the p-type γ-CuI and holes from the p-type γ-CuI to the n-type Cu_3N via the TiO_2 tunnel barrier. One could use, alternatively, h-BN as opposed to TiO_2 that contains oxygen. The previous explanation concerning the TiO_2 barrier is further corroborated by the fact that we obtained rectifying IV behavior from a γ-CuI/Cu_3N p-n heterojunction, as shown in Figure 8c. This γ-CuI/Cu_3N p-n heterojunction was fabricated by the deposition of n-type Cu_3N on SLG under Ar: 10% N_2 that was annealed at 400 °C for 30 min under NH_3: H_2. Half of the n-type Cu_3N layer was subsequently converted into p-type γ-CuI and the device completed with Au contacts.

To the best of our knowledge, no one has previously obtained rectifying IV characteristics from a p-n heterojunction consisting of n-type Cu_3N and γ-CuI. However, we did not observe any change in the IVs upon illumination. Our device is similar to that of Yee et al. [21], who fabricated an Al: ZnO/ZnS/Cu_3N p-n heterojunction on a 1 μm thick Mo film that was sputtered on SLG and used as a back contact. The n-type Cu_3N layer, which had a thickness of 350 nm, was deposited on the Mo by *rf* sputtering at 25 W and 160 °C under N_2. This was followed by a 50 nm ZnS n-type buffer layer that was deposited using atomic layer deposition at 125 °C. Next, 250 nm of Al: ZnO was deposited as the transparent top electrode, followed by the deposition of Al contacts having a thickness of 3 μm. However, the Cu_3N/ZnS p-n junction did not generate any photocurrent. The lack of photoconductivity and photo generated current in Cu_3N was explained by the large concentration of Cu_i defects that capture electrons and cause substantial Shockley–Read–Hall recombination, thereby quenching the steady-state minority carrier concentration under illumination. This may be one of the reasons why we did not observe a photocurrent in the γ-CuI/TiO_2/Cu_3N and γ-CuI/Cu_3N p-n heterojunction devices described above, while another contributing factor may be the occurrence of mid-gap states in the TiO_2 and γ-CuI that are detected in the PL and by UPPS. Nevertheless, the fabrication of γ-CuI/TiO_2/Cu_3N and γ-CuI/Cu_3N p-n heterojunctions with rectifying IV characteristics is an important step towards the realization of a solar cell using low cost, non-toxic semiconductor materials, such as Cu_3N, in combination with other wide band gap semiconductors, such as γ-CuI.

4. Conclusions

We deposited Cu_3N layers on f-SiO_2 by reactive sputtering under N_2, annealed them under NH_3: H_2 at 400 °C for 30 min and doped them with I_2. The I: Cu_3N layers have a cubic crystal structure, hole densities between 10^{16} and 10^{17} cm^{-3} and exhibited distinct spectral features at ~2.01 eV (≡617 nm) and 1.87 eV (≡660 nm) that correspond to the M and R direct energy band gaps of Cu_3N in excellent agreement with density functional theory calculations. The incorporation of iodine in Cu_3N gives rise to shallow-like acceptors, but no mid-gap states. However, the extended incorporation of iodine leads to the formation of γ-CuI along Cu_3N and an additional maximum in differential transmission at ~2.25 eV (≡550 nm) due to the formation of strained Cu_3N by the lattice expansion of γ-CuI. The Cu_3N was totally converted into γ-CuI, which had a hole density of 4×10^{17} cm^{-3}, mobility of 12 cm^2/Vs and showed a single maximum in differential transmission at ~2.95 eV, as observed by UPPS, consistent with the PL at 3.1 eV observed between 77 and 300 K that is very close to the fundamental direct energy band gap of CuI. We have demonstrated that n-type Cu_3N and γ-CuI may be used for the fabrication of γ-CuI/TiO_2/Cu_3N and Cu_3N/CuI p-n heterojunctions that exhibit rectifying IV properties. However, we did not observe any photocurrent due to the short lifetimes of photo generated electron-hole pairs

in Cu_3N attributed to Shockley–Read–Hall indirect recombination and/or mid-gap states in the γ-CuI and TiO_2. It is necessary then to find ways of increasing the lifetimes and diffusion lengths of carriers in both the Cu_3N and γ-CuI by increasing the crystal quality and/or by doping with suitable impurities.

Author Contributions: All of the authors performed research. M.Z. conceived the idea, designed and managed the research. A.T. worked on the growth, device fabrication and electrical characterization. A.O. performed optical spectroscopy. J.K. and T.P. worked on the theoretical calculations. M.Z. wrote the paper. All authors have read and agreed to the published version of the manuscript.

Funding: This research was co-financed by Greece and the European Union (European Social Fund-ESF) through the Operational Programme «Human Resources Development, Education and Lifelong Learning» in the context of the project "Reinforcement of Postdoctoral Researchers—2nd Cycle" (MIS-5033021), implemented by the State Scholarships Foundation (IKϒ). Computational resources were provided by the Greek Research & Technology Network (GRNET) in the "ARIS" National HPC infrastructure under the project NOUS (pr010034).

Conflicts of Interest: The authors declare no conflict of interest.

References

1. Zakutayev, A.; Caskey, C.M.; Fioretti, A.N.; Ginley, D.S.; Vidal, J.; Stevanovic, V.; Tea, E.; Lany, S. Defect Tolerant Semiconductors for Solar Energy Conversion. *J. Phys. Chem. Lett.* **2014**, *5*, 1117–1125. [CrossRef] [PubMed]
2. Dongsoo, L.; Seho, S.; Jiseok, K.; Hyunjung, P.; Minchul, J.; Eunkyung, P.; Byoungkuk, S.; Yeongil, J.; Taeseup, S.; Ungyu, P. Copper Nitride Nanowires Printed Li with Stable Cycling for Li Metal Batteries in Carbonate Electrolytes. *Adv. Mater.* **2020**, *32*, 1905573.
3. Birkett, M.; Savory, C.N.; Fioretti, A.N.; Thompson, P.; Muryn, C.A.; Weerakkody, A.D.; Mitrovic, I.Z.; Hall, S.; Treharne, R.; Dhanak, V.R.; et al. Atypically small temperature-dependence of the direct band gap in the metastable semiconductor copper nitrideCu_3N. *Phys. Rev. B* **2017**, *95*, 115201. [CrossRef]
4. Matsuzaki, K.; Harada, K.; Kumagai, Y.; Koshiya, S.; Kimoto, K.; Ueda, S.; Sasase, M.; Maeda, A.; Susaki, T.; Kitano, M.; et al. High-Mobility p-Type and n-Type Copper Nitride Semiconductors by Direct Nitriding Synthesis and In Silico Doping Design. *Adv. Mater.* **2018**, *30*, e1801968. [CrossRef]
5. Zervos, M.; Othonos, A.; Sergides, M.; Pavloudis, T.; Kioseoglou, J. Observation of the Direct Energy Band Gaps of Defect-Tolerant Cu_3N by Ultrafast Pump-Probe Spectroscopy. *J. Phys. Chem. C* **2020**, *124*, 3459–3469. [CrossRef]
6. Nikam, R.D.; Kwak, M.; Lee, J.; Rajput, K.G.; Banerjee, W.; Hwang, H. Near ideal synaptic functionalities in Li ion synaptic transistor using $Li_3POxSex$ electrolyte with high ionic conductivity. *Sci. Rep.* **2019**, *9*, 1–11. [CrossRef]
7. Kozen, A.C.; Pearse, A.J.; Lin, C.-F.; Noked, M.; Rubloff, G.W. Atomic Layer Deposition of the Solid Electrolyte LiPON. *Chem. Mater.* **2015**, *27*, 5324–5331. [CrossRef]
8. Yamada, N.; Ino, R.; Ninomiya, Y. Truly Transparent p-Type γ-CuI Thin Films with High Hole Mobility. *Chem. Mater.* **2016**, *28*, 4971–4981. [CrossRef]
9. Yamada, N.; Kondo, Y.; Ino, R. Low-Temperature Fabrication and Performance of Polycrystalline CuI Films as Transparent p-Type Semiconductors. *Phys. Status Solidi* **2019**, *216*, 1700782. [CrossRef]
10. Sepalage, G.A.; Meyer, S.; Pascoe, A.; Scully, A.D.; Huang, F.; Bach, U.; Cheng, Y.B.; Spiccia, L. Copper(I) Iodide as Hole-Conductor in Planar Perovskite Solar Cells: Probing the Origin of J–V Hysteresis. *Adv. Funct. Mater.* **2015**, *25*, 5650–5661. [CrossRef]
11. Sun, W.; Peng, H.; Li, Y.; Yan, W.; Liu, Z.; Bian, Z.; Huang, C. Solution-Processed Copper Iodide as an Inexpensive and Effective Anode Buffer Layer for Polymer Solar Cells. *J. Phys. Chem. C* **2014**, *118*, 16806–16812. [CrossRef]
12. Zainun, A.R.; Mamat, M.H.; Noor, U.M.; Rusop, M. Particles Size and Conductivity Study of P-Type Copper (I) Iodide (CuI) Thin Film for Solid State Dye-Sensitized Solar Cells. *IOP Conf. Ser. Mater. Sci. Eng.* **2011**, *17*, 012009. [CrossRef]
13. Jeona, K.; Jeea, H.; Parka, M.J.; Limb, S.; Jeonga, C. Characterization of the Copper Iodide Hole-Selective Contact for Silicon Solar Cell Application. *Thin Solid Films* **2018**, *660*, 613–617. [CrossRef]
14. Luo, W.; Zeng, C.; Du, X.; Leng, C.; Yao, W.; Shi, H.; Wei, X.; Du, C.; Lu, S. Copper thiocyanate/copper iodide based hole transport composites with balanced properties for efficient polymer light-emitting diodes. *J. Mater. Chem. C* **2018**, *6*, 4895–4902. [CrossRef]
15. Choi, C.-H.; Gorecki, J.Y.; Fang, Z.; Allen, M.; Li, S.; Lin, L.-Y.; Cheng, C.-C.; Chang, C.-H. Low-temperature, inkjet printed p-type copper(I) iodide thin film transistors. *J. Mater. Chem. C* **2016**, *4*, 10309–10314. [CrossRef]
16. Bai, S.-Q.; Wong, I.H.K.; Lin, M.; Young, D.J.; Hor, T.S.A. A thermoelectric copper-iodide composite from the pyrolysis of a well-defined coordination polymer. *Dalton Trans.* **2018**, *47*, 5564–5569. [CrossRef] [PubMed]
17. Revan, D.N.; Ashok, S.P.; Sankar, R.; Chen, Y.T. Epitaxial Growth of Vertically Stacked p-MoS_2/n-MoS_2. *Nano Energy* **2017**, *32*, 454–462.
18. Bartolomeo, A. Emerging 2D Materials and Their Van Der Waals Heterostructures. *Nanomaterials* **2020**, *10*, 579. [CrossRef]
19. Gibertini, M.; Koperski, M.; Morpurgo, A.F.; Novoselov, K.S. Magnetic 2D Materials and Heterostructures. *Nat. Nanotechnol.* **2019**, *14*, 408. [CrossRef] [PubMed]

20. Chen, S.-C.; Huang, S.-Y.; Sakalley, S.; Paliwal, A.; Chen, Y.-H.; Liao, M.-H.; Sun, H.; Biring, S. Optoelectronic properties of Cu_3N thin films deposited by reactive magnetron sputtering and its diode rectification characteristics. *J. Alloys Compd.* **2019**, *789*, 428–434. [CrossRef]
21. Yee, Y.S.; Inoue, H.; Hultqvist, A.; Hanifi, D.; Salleo, A.; Magyari-Köpe, B.; Nishi, Y.; Bent, S.F.; Clemens, B.M. Copper interstitial recombination centers in Cu_3N. *Phys. Rev. B* **2018**, *97*, 245201. [CrossRef]
22. Yu, A.; Hu, R.; Liu, W.; Zhang, R.; Zhang, J.; Pu, Y.; Chu, L.; Yang, J.; Li, X. Preparation and characterization of Mn doped copper nitride films with high photocurrent response. *Curr. Appl. Phys.* **2018**, *18*, 1306–1312. [CrossRef]
23. Kresse, G.; Furthmüller, G. Efficiency of Ab-Initio Total Energy Calculations for Metals and Semiconductors Using a Plane-Wave Basis Set. *Comput. Mater. Sci.* **1996**, *6*, 15–50. [CrossRef]
24. Kresse, G.; Furthmüller, G. Efficient Iterative Schemes for Ab Initio Total-Energy Calculations Using a Plane-Wave Basis Set. *Phys. Rev. B* **1996**, *54*, 11169. [CrossRef] [PubMed]
25. Blochl, P.E. Projector Augmented-Wave Method. *Phys. Rev. B* **1994**, *50*, 17953. [CrossRef] [PubMed]
26. Kresse, G.; Joubert, D. From Ultra Soft Pseudopotentials to the Projector Augmented-Wave Method. *Phys. Rev. B* **1999**, *59*, 1758–1775. [CrossRef]
27. Perdew, J.P.; Burke, K.; Ernzerhof, M. Generalized gradient approximation made simple. *Phys. Rev. Lett.* **1997**, *77*, 3865–3868. [CrossRef] [PubMed]
28. Dudarev, S.L.; Botton, G.A.; Savrasov, S.Y.; Humphreys, C.J.; Sutton, A.P. Electron-energy-loss spectra and the structural stability of nickel oxide: An LSDA+U study. *Phys. Rev. B* **1998**, *57*, 1505–1509. [CrossRef]
29. Freysoldt, C.; Grabowski, B.; Hickel, T.; Neugebauer, J.; Kresse, G.; Janotti, A.; Van de Walle, C.G. First-principles calculations for point defects in solids. *Rev. Mod. Phys.* **2014**, *86*, 253–305. [CrossRef]
30. Zervos, M.; Othonos, A.; Pavloudis, T.; Giaremis, S.; Kioseoglou, J.; Mavridou, K.; Katsikini, M.; Pinakidou, F.; Paloura, E.C. Impact of Oxygen on the Properties of Cu_3N and $Cu_{3-x}N_{1-}xO_x$. *J. Phys. Chem. C* **2021**, *125*, 3680–3688. [CrossRef]
31. Peng, Y.; Yaacobi-Gross, N.; Perumal, A.K.; Faber, H.; Vourlias, G.; Patsalas, P.A.; Bradley, D.D.C.; He, Z.; Anthopoulos, T. Efficient organic solar cells using copper(I) iodide (CuI) hole transport layers. *Appl. Phys. Lett.* **2015**, *106*, 243302. [CrossRef]
32. Gotoha, K.; Cuia, M.; Takahashia, I.; Kurokawaa, Y.; Usamia, N. Development of Spin-Coated Copper Iodide on Silicon for use in Hole-Selective Contacts. *Energy Procedia* **2017**, *124*, 598–603. [CrossRef]
33. Kumarasinghe, A.R.; Flavell, W.R.; Thomas, A.G.; Mallick, A.K.; Tsoutsou, D.; Chatwin, C.; Rayner, S.; Kirkham, P.; Warren, S.; Patel, S.; et al. Electronic Properties of the Interface between *p*-CuI and Anatase-Phase *n*-TiO_2 Single Crystal and Nanoparticulate Surfaces: A Photoemission Study. *J. Chem. Phys.* **2007**, *127*, 114703. [CrossRef] [PubMed]